Electronic Supplementary Information

Naphthyridine-based thermally activated delayed fluorescence emitters for multi-color organic light-emitting diodes with low efficiency roll-off

Cheng Chen,[a] Hai-Yan Lu,*[,a] Yin-Feng Wang,[a] Meng Li,[b] Yi-Fan Shen,[a] and Chuan-Feng Chen*[,a, b]

[a]*University of Chinese Academy of Sciences, Beijing 100049, China*. [b]*Beijing National Laboratory for Molecular Sciences, CAS Key Laboratory of Molecular Recognition and Function, Institute of Chemistry, Chinese Academy of Sciences, Beijing 100190, China.*

E-mail: haiyanlu@ucas.ac.cn; cchen@iccas.ac.cn

Contents

1. General information

All the reagents and solvents were purchased from commercial sources and used without further purification. ^{1}H and ^{13}C NMR spectra were recorded on AVIII 400 MHz NMR spectrometers in $CDCl_3$ solutions. High resolution mass spectra were measured on a Thermo Fisher® Exactive high resolution LC-MS spectrometer. The calculation was carried out with the Gaussian 09 software package. Geometry optimizations were conducted under the M06-2X/6-31g(d,p) level of theory. Keyword 5d/7f was used in geometry optimization. Crystal structures were solved with direct methods and refined with a full-matrix least-squares technique, using the SHELXS software package. Thermal gravimetric analysis (TGA) were performed on a TA Instruments TGA 2050 thermal analyzer at a heating rate of 10 ℃ min^{-1} in nitrogen. Cyclic voltammetry was performed using a CHI600A analyzer with a scan rate of 100 mV/s at room temperature to investigate the reduction and oxidation potentials. A conventional three-electrode cell was used as electrolytic cell with a glassy carbon working electrode, an Ag/Ag^{+} (0.01 M $AgNO_3$) as the reference electrode, and Pt wire as the counter electrode. The oxidation potential was measured in CH_2Cl_2 with 0.1 M of tetra-n-butylammonium hexafluorophosphate (n-Bu_4NPF_6) as a supporting electrolyte. The UV-vis spectra were recorded on PerkinElmer® UV/Vis/NIR spectrometer (Lambda 950), and the fluorescence spectra were recorded on HITACHI® F-7000 Fluorescence Spectrometer at room temperature. The transient photoluminance decay characteristics and temperature dependence experiments and Absolute PL quantum yield, measured by Edinburgh FLS980 Spectrometer Device Fabrication and Measurement Devices were fabricated by vacuum deposition onto pre-coated ITO glass substrates with sheet resistance of 15 Ω/square at a pressure lower than 1×10^{-5} mbar for organic and metal deposition. Before the fabrication of devices, the ITO glass substrates were cleaned with Decon 90, rinsed in ultrapure water and ethanol, dried in an oven at 120 ℃, by plasma cleaning process. The devices were fabricated by evaporating organic onto the ITO glass substrates sequentially with an evaporation rate of 0.5~2 Å s^{-1}. LiF and Al were subsequently deposited as the cathode at a deposition rate of 0.1 Å s^{-1} and 5 Å s^{-1}, respectively. EL luminescence spectra and CIE color coordinates were measured with a Spectrascan PR650 photometer, and the current-voltage characteristics were measured with a computer-controlled Keithley 2400 Source Meter under ambint atmosphere.

2. X-ray crystallographic data

Table S1. Crystal data and structure refinement for **PTZ-ND**

Empirical formula	C_{32} H_{20} N_4 S_2	
CCDC No.	1893131	
Formula weight	524.64	
Temperature	173.15 K	
Wavelength	1.54178 Å	
Crystal system	Orthorhombic	
Space group		
P n m a		
Unit cell dimensions	a = 8.18250(10) Å	α= 90 °.
	b = 27.5249(2) Å	β= 90 °.
	c = 12.85110(10) Å	γ = 90 °.
Volume	2894.36(5) $Å^3$	
Z	4	
Density (calculated)	1.204 Mg/m^3	
Absorption coefficient	1.869 mm^{-1}	
F(000)	1088	
Crystal size	0.352 x 0.323 x 0.311 mm^3	
Theta range for data collection	3.211 to 75.577 °.	
Index ranges	-10<=h<=9, -34<=k<=33, -14<=l<=16	
Reflections collected	24727	
Independent reflections	2965 [R(int) = 0.0253]	
Completeness to theta = 67.679 °	99.9 %	
Absorption correction	Semi-empirical from equivalents	
Max. and min. transmission	1.000 and 0.7169	
Refinement method	Full-matrix least-squares on F^2	
Data / restraints / parameters	2965 / 0 / 175	
Goodness-of-fit on F^2	1.112	
Final R indices [I>2sigma(I)]	R1 = 0.0418, wR2 = 0.1086	
R indices (all data)	R1 = 0.0422, wR2 = 0.1089	
Extinction coefficient	n/a	
Largest diff. peak and hole	0.460 and -0.395 $e.Å^{-3}$	

Table S2. Crystal data and structure refinement for **DMAC-ND**

Empirical formula	$C_{38}H_{32}N_4$	
CCDC No.	1893132	
Formula weight	544.67	
Temperature	169.99(10) K	
Wavelength	1.54184 Å	
Crystal system	Orthorhombic	
Space group	P 21 21 21	
Unit cell dimensions	a = 9.03220(10) Å	α= 90 °.
	b = 12.26750(10) Å	β= 90 °.
	c = 25.1471(4) Å	γ = 90 °.
Volume	2786.36(6) $Å^3$	
Z	4	
Density (calculated)	1.298 Mg/m^3	
Absorption coefficient	0.593 mm^{-1}	
F(000)	1152	
Crystal size	0.245 x 0.213 x 0.031 mm^3	
Theta range for data collection	3.515 to 75.469 °.	
Index ranges	-10<=h<=10, -5<=k<=14, -29<=l<=31	
Reflections collected	18177	
Independent reflections	5482 [R(int) = 0.0277]	
Completeness to theta = 67.684 °	99.8 %	
Absorption correction	Semi-empirical from equivalents	
Max. and min. transmission	1.00000 and 0.59976	
Refinement method	Full-matrix least-squares on F^2	
Data / restraints / parameters	5482 / 0 / 383	
Goodness-of-fit on F^2	1.074	
Final R indices [I>2sigma(I)]	R1 = 0.0357, wR2 = 0.0900	
R indices (all data)	R1 = 0.0408, wR2 = 0.0973	
Absolute structure parameter	-0.14(17)	
Extinction coefficient	n/a	
Largest diff. peak and hole	0.212 and -0.163 $e.Å^{-3}$	

Table S3. Crystal data and structure refinement for **PXZ-ND**

Empirical formula	$C_{32}\ H_{20}\ N_4\ O_2$	
CCDC No.	1893133	
Formula weight	492.52	
Temperature	169.99(10) K	
Wavelength	1.54184 Å	
Crystal system	Monoclinic	
Space group	P 1 21 1	
Unit cell dimensions	a = 9.84880(10) Å	α= 90 °.
	b = 7.41860(10) Å	β= 104.8480(10) °.
	c = 16.2441(2) Å	γ = 90 °.
Volume	1147.23(2) $Å^3$	
Z	2	
Density (calculated)	1.426 Mg/m^3	
Absorption coefficient	0.730 mm^{-1}	
F(000)	512	
Crystal size	0.3 x 0.15 x 0.1 mm^3	
Theta range for data collection	2.814 to 75.158 °.	
Index ranges	-12<=h<=11, -8<=k<=8, -20<=l<=20	
Reflections collected	21203	
Independent reflections	4517 [R(int) = 0.0236]	
Completeness to theta = 67.684 °	99.9 %	
Absorption correction	Semi-empirical from equivalents	
Max. and min. transmission	1.00000 and 0.77008	
Refinement method	Full-matrix least-squares on F^2	
Data / restraints / parameters	4517 / 1 / 343	
Goodness-of-fit on F^2	1.067	
Final R indices [I>2sigma(I)]	R1 = 0.0320, wR2 = 0.0803	
R indices (all data)	R1 = 0.0325, wR2 = 0.0810	
Absolute structure parameter	0.04(4)	
Extinction coefficient	n/a	
Largest diff. peak and hole	0.114 and -0.250 $e.Å^{-3}$	

3. Schematic molecular conformations and interactions

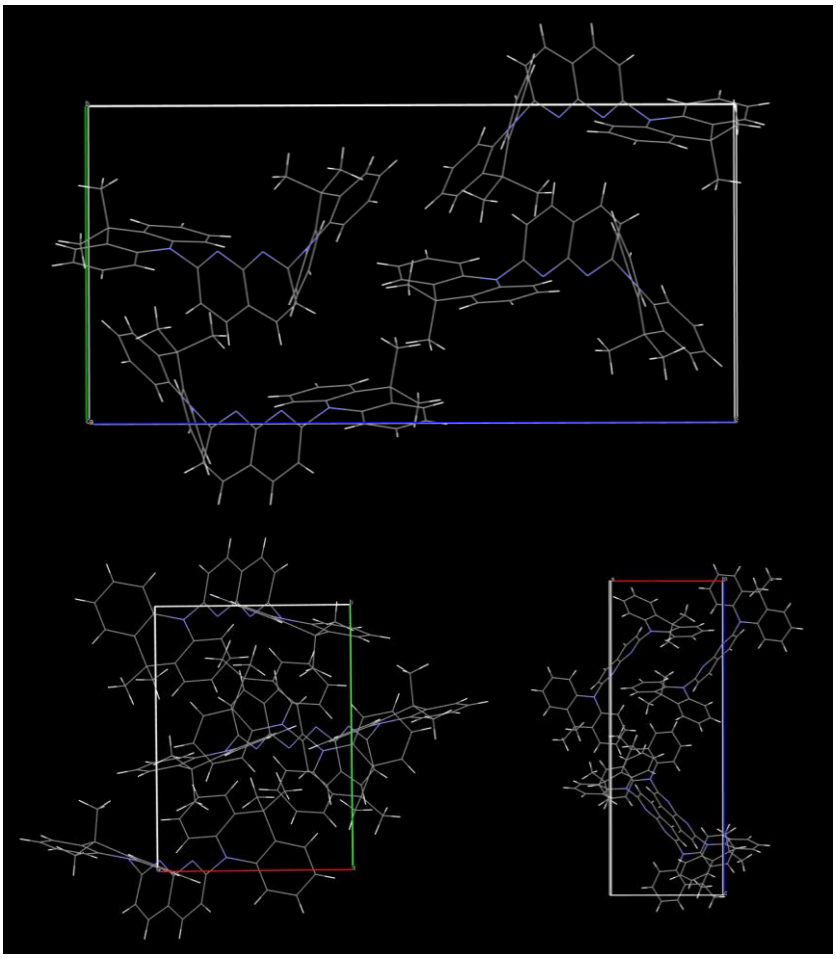

Fig. S1. Schematic molecular conformations and interactions in the crystal structure of **DMAC-ND**.

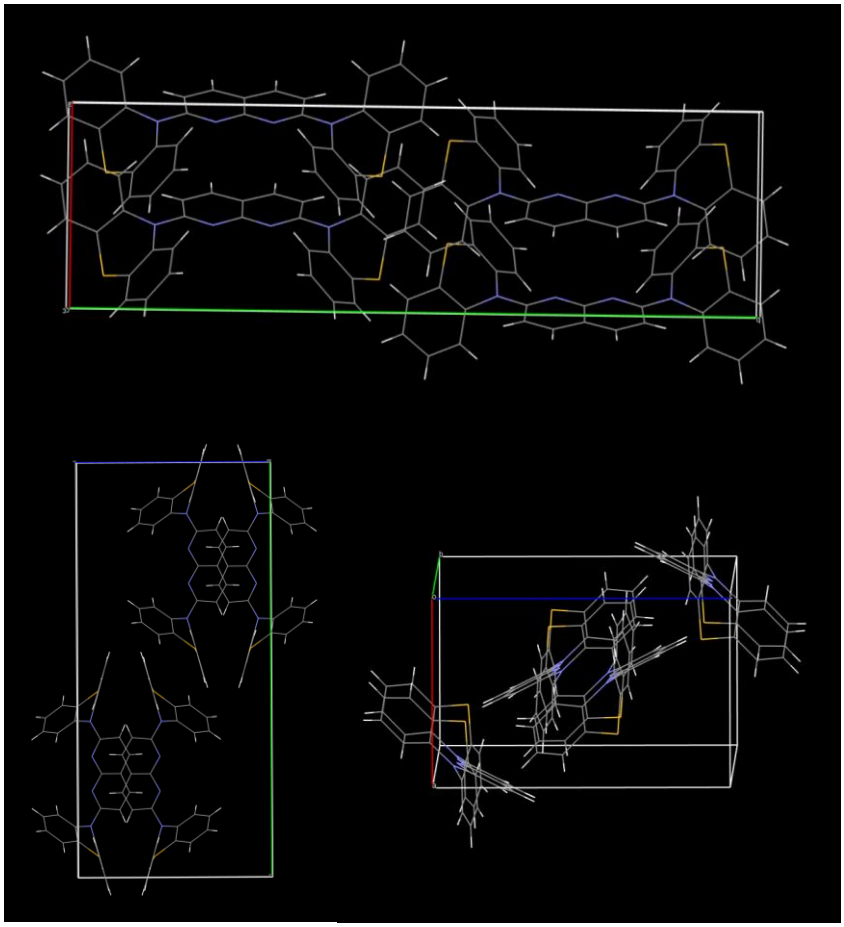

Fig. S2. Schematic molecular conformations and interactions in the crystal structure of **PTZ-ND**.

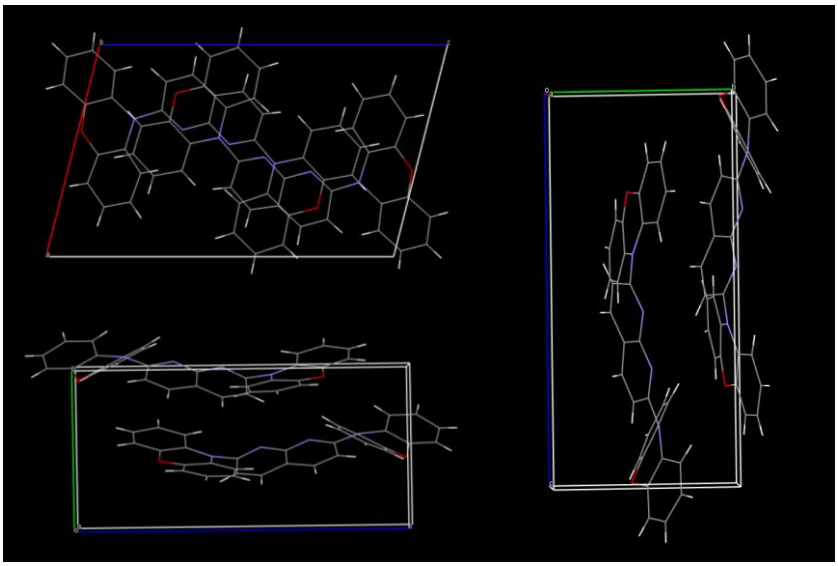

Fig. S3. Schematic molecular conformations and interactions in the crystal structure of **PXZ-ND**.

4. DFT calculations

The ground state geometries of three molecules are optimized by density functional theory (DFT) using the B3LYP functional. In order to investigate the energies and the transition characters of the low-lying excited singlet and triplet states, time-dependent density functional theory (TDDFT) with B3LYP functional, was used to calculate the vertical excitation energies for S_1 and T_1 as well as ΔE_{ST}. All the above calculations were carried out by using Gaussian 09 with the 6-31G** basis set.[S1]

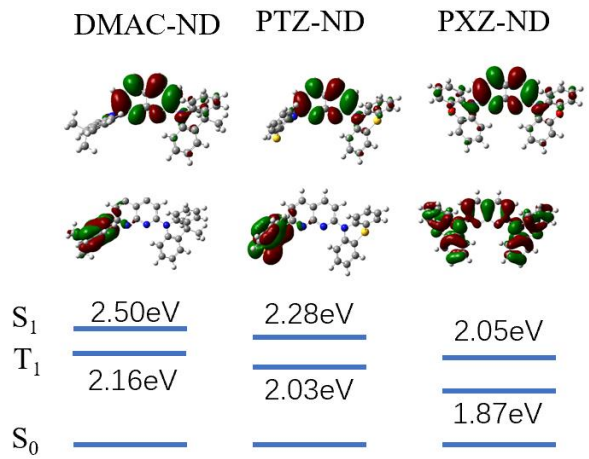

Fig. S4 Energy diagram of calculated singlet and triplet excited states for **DMAC-ND**, **PTZ-ND** and **PXZ-ND**.

5. TGA and DSC

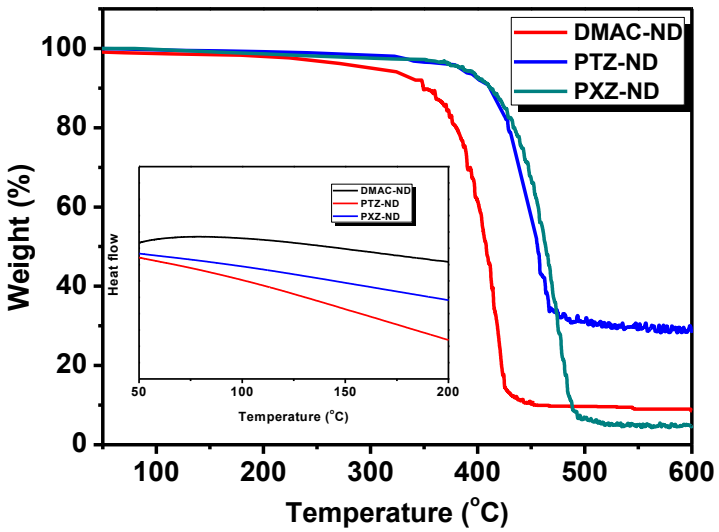

Fig. S5. TGA traces of **DMAC-ND**, **PTZ-ND** and **PXZ-ND** at a heating rate of 10 ^{o}C min^{-1}. Inset: DSC traces of **DMAC-ND**, **PTZ-ND** and **PXZ-ND** at a heating rate of 10 ^{o}C min^{-1}.

6. Photophysical properties

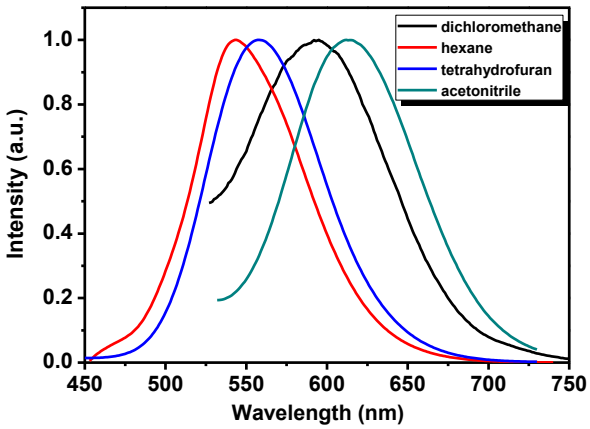

Fig. S6. FL spectra of **DMAC-ND** in different solvents (1×10^{-5} M).

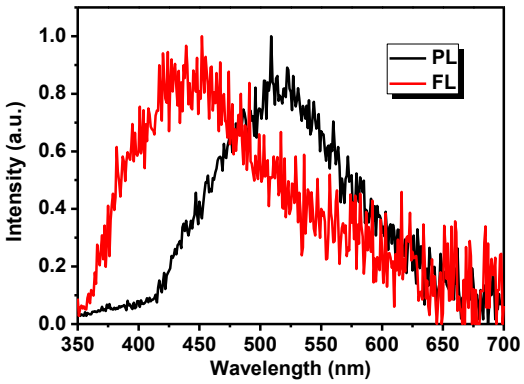

Fig. S7. Normalized photoluminescence and phosphorescence spectra of 1,8-**ND** in neat films at 77K.

Table S4. Physical properties of 1,8-**ND** in neat films

λ_{FL}[a]	λ_{Phos}[b]	E_{S1}[c]	E_{T1}[d]	ΔE_{ST}[e]
441 nm	516 nm	2.81 eV	2.40 eV	0.41 eV

[a]Fluorescence and [b]phosphorescence emission peaks measured at 77 K. [c]S_1 and [d]T_1 energy levels ($\approx 1240/\lambda$). [e]$\Delta E_{ST} = E_{S1}-E_{T1}$.

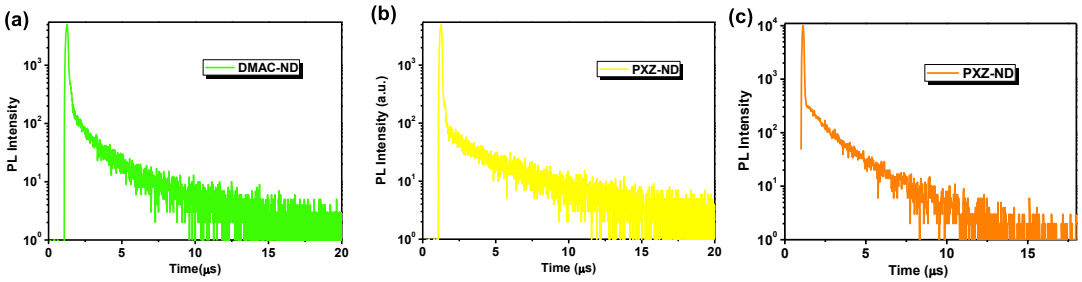

Fig. S8. Transient PL spectra of (a) **DMAC-ND**, (b) **PTZ-ND** and (c) **PXZ-ND** doped into mCP films (5 wt%) at 300 K.

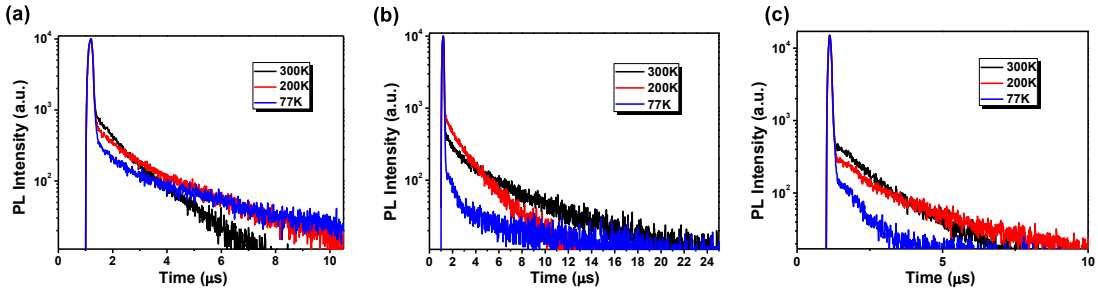

Fig. S9. Transient PL spectra of (a) **DMAC-ND**, (b) **PTZ-ND**, and (c) **PXZ-ND** doped into mCP films (3 wt%) from 100 to 300 K.

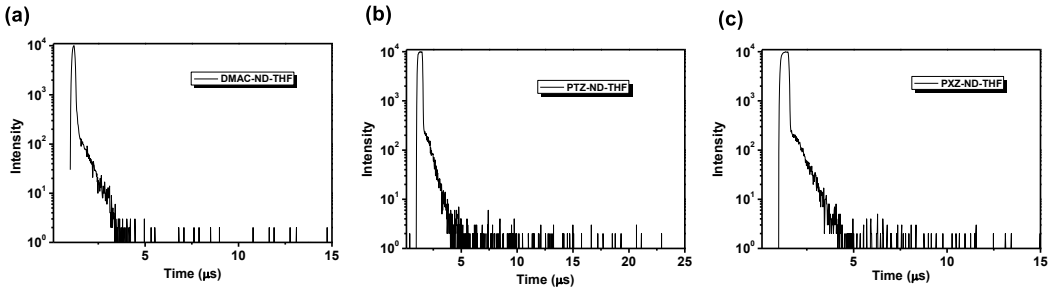

Fig. S10. Transient PL spectra of (a) **DMAC-ND**, (b) **PTZ-ND** and (c) **PXZ-ND** in THF solution at 300 K.

7. Device fabrication and characterization

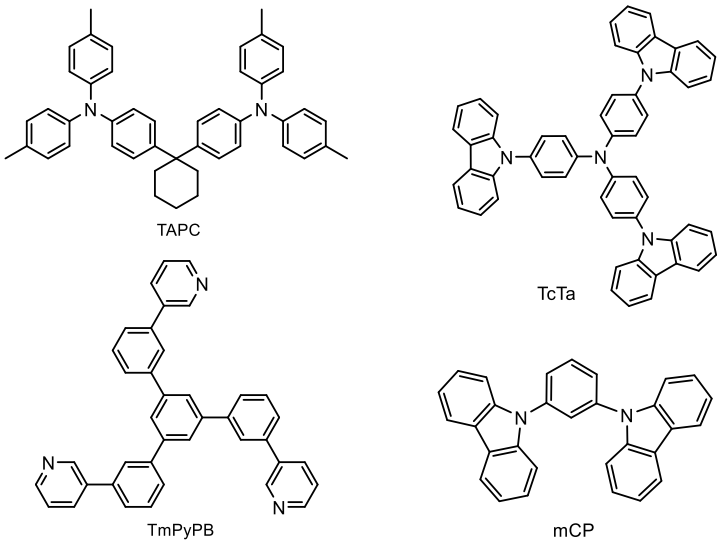

Fig. S11. Molecular structures of the compounds used in the devices.

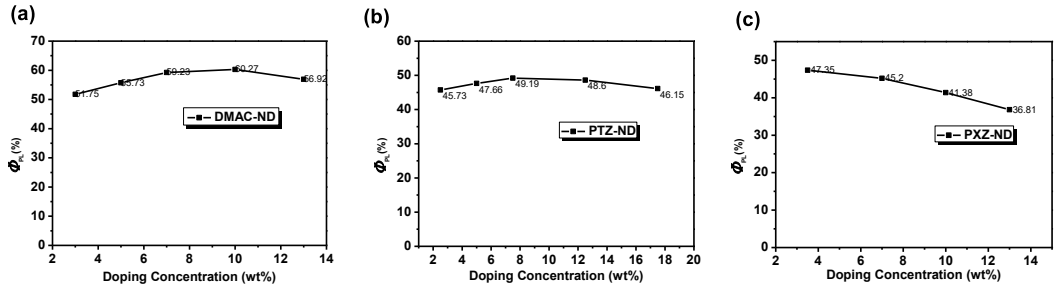

Fig. S12. Φ_{PL} versus doping concentration of (a) **DMAC-ND**, (b) **PTZ-ND** and (c) **PXZ-ND** doped in mCP films.

Table S5. The summary of best EL characteristics for **DMAC-ND** with different host materials.

Host material	V_{on}^{a} (V) [a]	EQE [b] (%)	PE [c] (lm/W)	CE [d] (cd/A)
CBP	7.2	9.92	10.11	31.54
mCP	3.1	14.10	36.90	38.11
mCBP	3.7	8.90	16.65	21.20

[a] The turn-on voltage recorded at a brightness of 1 cd/m^2. [b] Maximal external quantum efficiency. [c] Maximal power efficiency. [d] Maximal current efficiency.

Table S6. The summary of EL characteristics for **DMAC-ND**, **PTZ-ND** and **PXZ-ND** with different concentration in mCP.

	Concentration (wt %)	V_{on}^{a} (V) [a]	EQE [b] (%)	PE [c] (lm/W)	CE [d] (cd/A)
DMAC-ND	3	3.4	10.1	21.3	25.1
	5	3.4	11.4	26.4	27.7
	7	3.2	13.1	28.5	33.6
	10	3.1	14.1	36.9	38.1
	13	3.2	11.8	29.6	30.1
PTZ-ND	2.5	3.6	10.6	27.0	31.8
	5	3.6	11.7	29.0	34.1
	7.5	3.4	13.0	31.4	40.9
	12	3.5	12.3	32.9	37.7
	17.5	3.6	11.2	29.0	34.2
PXZ-ND	3.5	3.0	13.4	30.7	43.2
	7	3.1	12.4	29.8	40.1
	10	3.1	11.1	30.7	35.2
	13	3.1	9.8	28.8	31.1

[a] The turn-on voltage recorded at a brightness of 1 cd/m^2. [b] Maximal external quantum efficiency. [c] Maximal power efficiency. [d] Maximal current efficiency.

8. Estimation of basic photophysical data

Table S7. Transient PL decay data of **DMAC-ND**, **PTZ-ND** and **PXZ-ND** in neat films in 300K[a].

compound	τ_{PF} (ns)	τ_{DF} (ns)	Φ_{PLQY} (%)	Φ_{PF} (%)	k_F (10^6 s^{-1})	k_{IC} (10^6 s^{-1})	k_{ISC} (10^6 s^{-1})	Φ_{ISC} (%)	k_{RISC} (10^6 s^{-1})
DMAC-ND	63	1372	40.8	15.2	2.4	3.6	9.8	62.1	1.90
PTZ-ND	37	1262	36.0	7.6	2.0	3.7	21.3	78.8	1.38
PXZ-ND	28	972	13.4	8.3	2.9	19.0	13.0	54.0	3.10

The two fluorescent lifetimes (τ_{PF} and τ_{DF}) can be revealed by fitting the decay curve of the time-resolved PL spectrum. Φ_{PF} is the quantum yields of prompt and delay fluorescence.

9. ^{1}H NMR and ^{13}C NMR spectra of new compounds

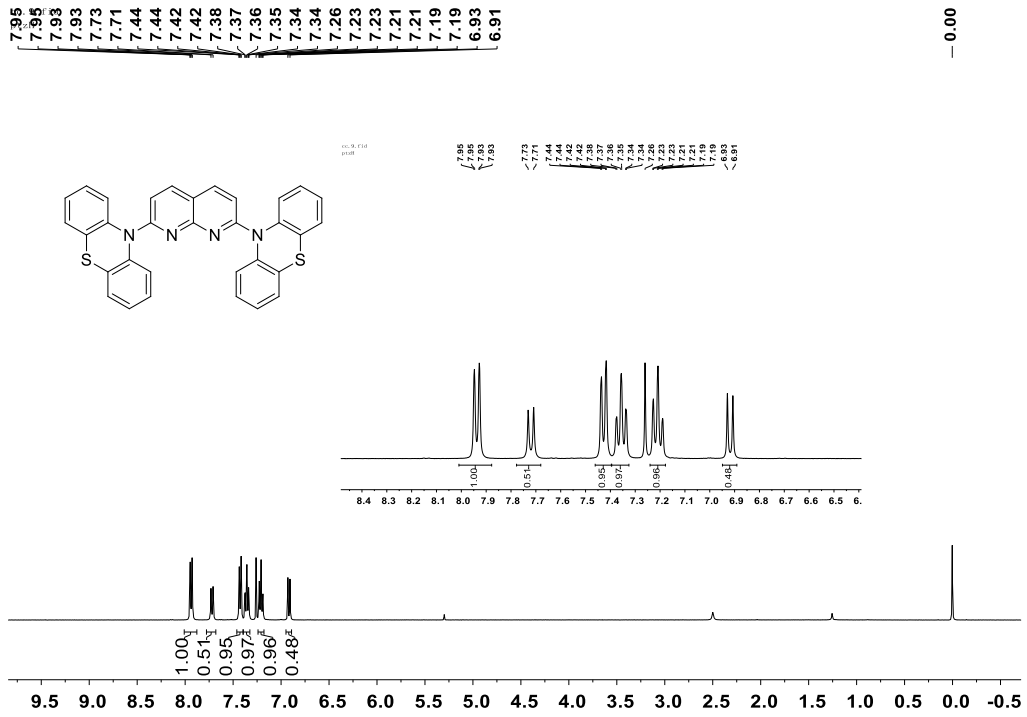

Fig. S13 ^{1}H NMR spectrum (400 MHz, $CDCl_3$, 300K) of **PTZ-ND**.

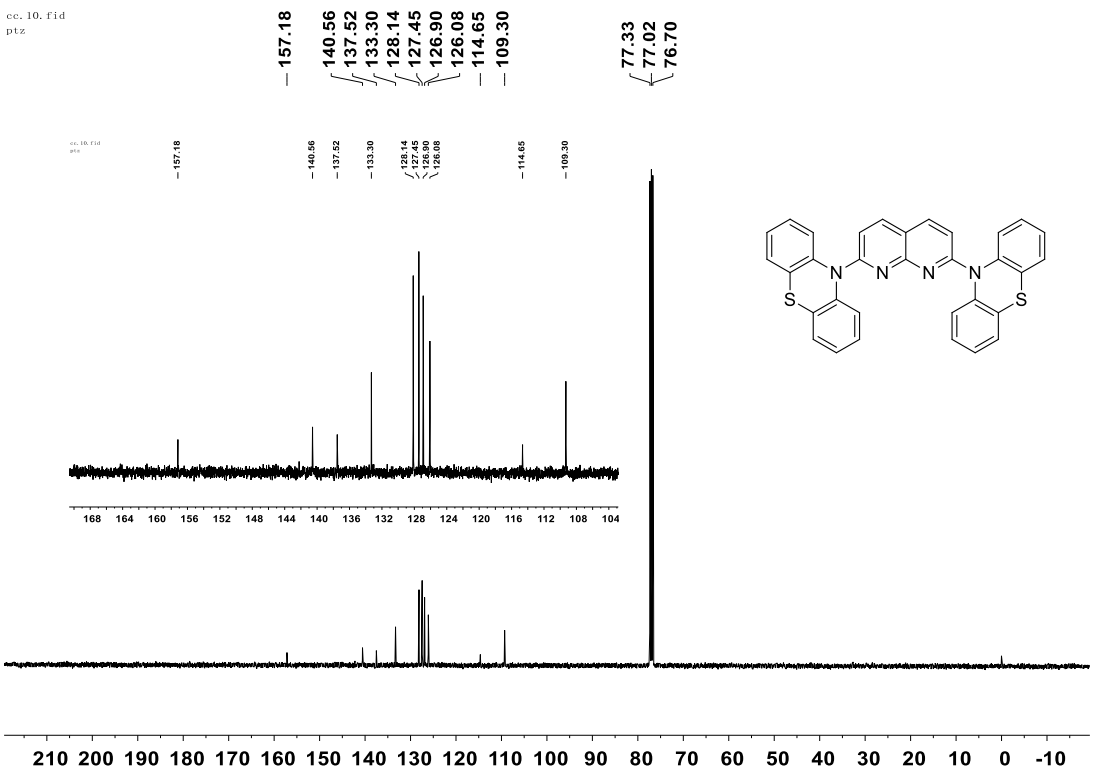

Fig. S14 ^{13}C NMR spectrum (101 HMz, $CDCl_3$, 300K) of **PTZ-ND**.

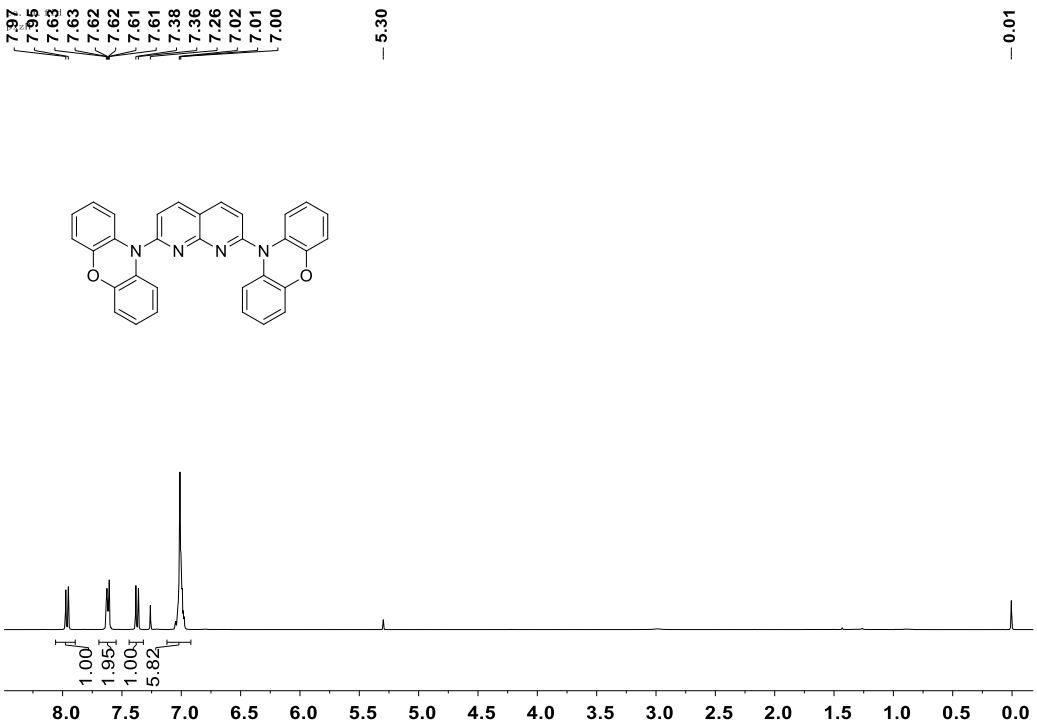

Fig. S15 ^{1}H NMR spectrum (400 MHz, $CDCl_3$, 300K) of **PXZ-ND**.

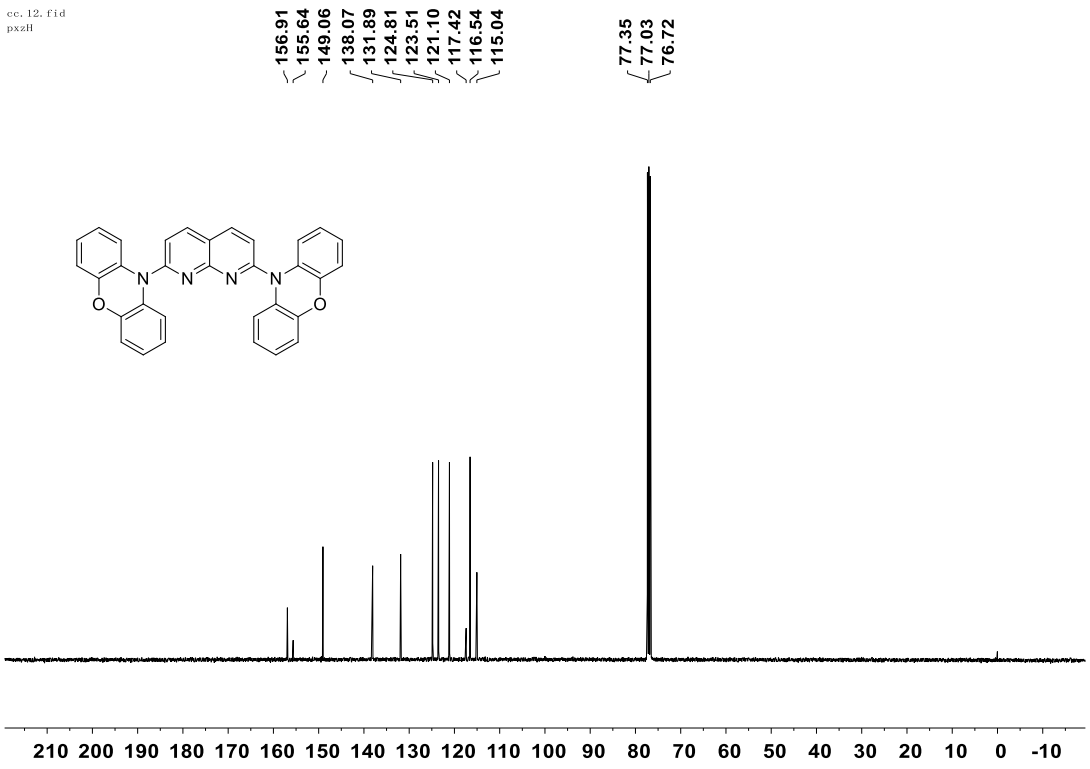

Fig. S16 ^{13}C NMR spectrum (101 HMz, $CDCl_3$, 300K) of **PXZ-ND**.

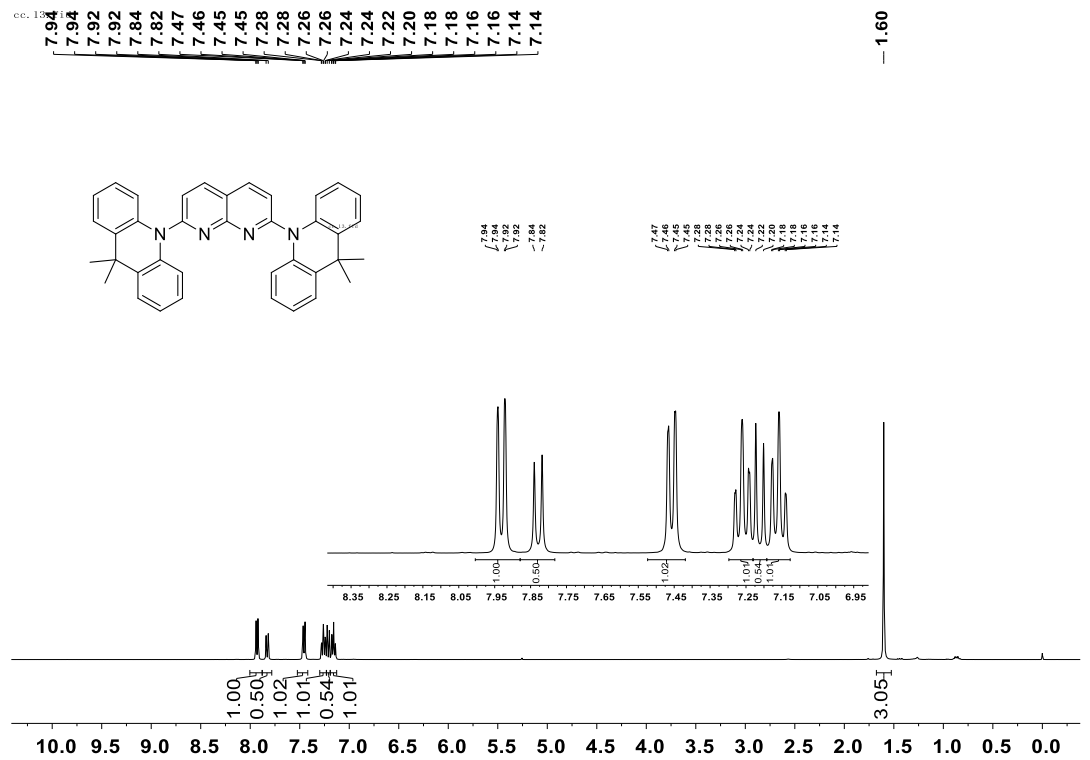

Fig. S17. ^{1}H NMR spectrum (400 MHz, $CDCl_3$, 300K) of **DMAC-ND**.

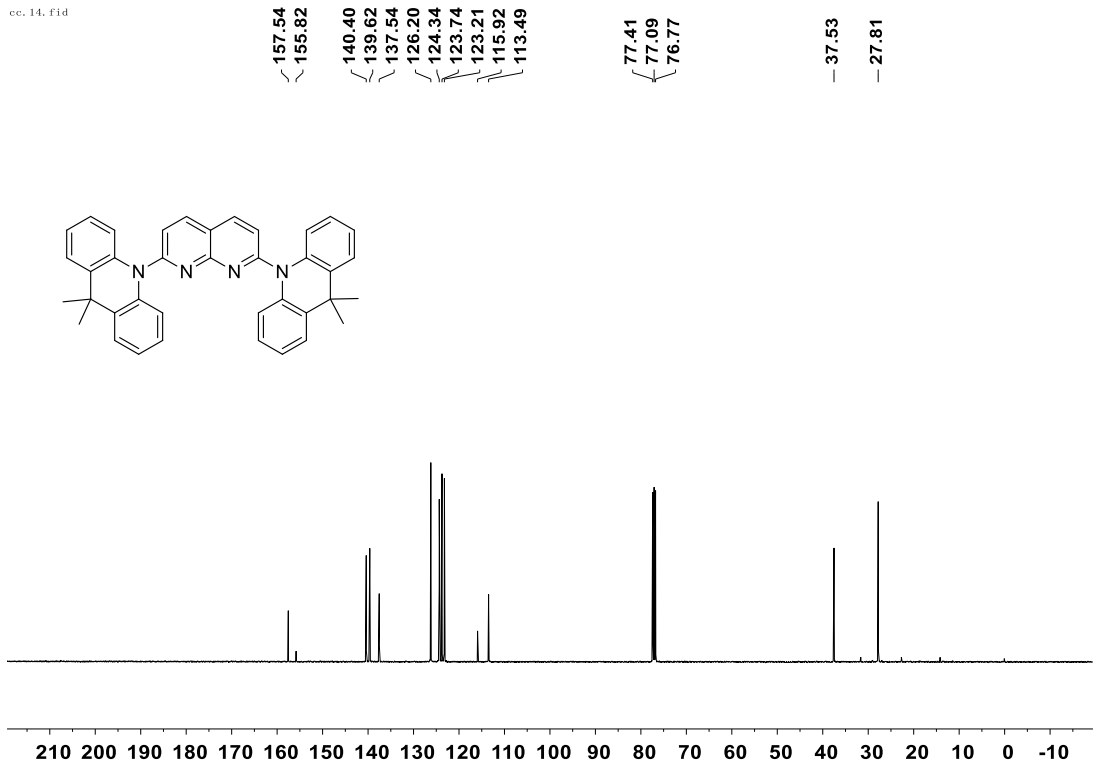

Fig. S18 ^{13}C NMR spectrum (101 HMz, $CDCl_3$, 300K) of **DMAC-ND**.

10. Reference

S1. Gaussian 09, Revision D.01, M. J. Frisch, G. W. Trucks, H. B. Schlegel, G. E. Scuseria, M. A. Robb, J. R. Cheeseman, G. Scalmani, V. Barone, B. Mennucci, G. A. Petersson, H. Nakatsuji, M. Caricato, X. Li, H. P. Hratchian, A. F. Izmaylov, J. Bloino, G. Zheng, J. L. Sonnenberg, M. Hada, M. Ehara, K. Toyota, R. Fukuda, J. Hasegawa, M. Ishida, T. Nakajima, Y. Honda, O. Kitao, H. Nakai, T. Vreven, J. A. Montgomery, Jr., J. E. Peralta, F. Ogliaro, M. Bearpark, J. J. Heyd, E. Brothers, K. N. Kudin, V. N. Staroverov, T. Keith, R. Kobayashi, J. Normand, K. Raghavachari, A. Rendell, J. C. Burant, S. S. Iyengar, J. Tomasi, M. Cossi, N. Rega, J. M. Millam, M. Klene, J. E. Knox, J. B. Cross, V. Bakken, C. Adamo, J. Jaramillo, R. Gomperts, R. E. Stratmann, O. Yazyev, A. J. Austin, R. Cammi, C. Pomelli, J. W. Ochterski, R. L. Martin, K. Morokuma, V. G. Zakrzewski, G. A. Voth, P. Salvador, J. J. Dannenberg, S. Dapprich, A. D. Daniels, O. Farkas, J. B. Foresman, J. V. Ortiz, J. Cioslowski, and D. J. Fox, Gaussian, Inc., Wallingford CT, **2013**.